PHYSICAL REVIEW C VOLUME 56, NUMBER 5 NOVEMBER 1997

Charm quark production in noncentral heavy ion collisions

V. Emel'yanov,[1] A. Khodinov,[1] S. R. Klein,[2] and R. Vogt[2,3]
[1]*Moscow State Engineering Physics Institute (Technical University), Kashirskoe Avenue 31, Moscow, 115409, Russia*
[2]*Nuclear Science Division, Lawrence Berkeley National Laboratory, Berkeley, California 94720*
[3]*Physics Department, University of California, Davis, California 95616*

(Received 23 June 1997)

The effect of gluon shadowing on charm quark production in large impact parameter ultrarelativistic heavy ion collisions is investigated. Charm quark production cross sections are calculated for a range of noncentral impact parameters which can be determined from the global transverse energy distribution. We show that charm quark production is a good probe of the local parton density which determines the effectiveness of shadowing. We discuss why shadowing may have a spatial dependence and show that this spatial dependence may be detected in noncentral heavy ion collisions. [S0556-2813(97)03211-1]

PACS number(s): 25.75.Dw, 21.65.+f, 24.85.+p

I. INTRODUCTION

Deep-inelastic scattering experiments using nuclear targets showed that the quark and antiquark distribution functions are modified in the nuclear environment [1] and hence are different in heavy nuclei than in free protons. It is not unreasonable to expect the nuclear gluon distributions to be affected at least as much as the quark distributions. However, little is known about the nuclear gluon distribution because the gluon distributions can only be indirectly probed. Gluon-dominated production processes, such as J/ψ and heavy quark production, can provide an indirect measure of the nuclear gluon distribution. Since the J/ψ is more strongly affected by absorption processes than charm quarks, evident from their respective A dependences [2,3], charm quark production provides a cleaner determination of the nuclear gluon distribution.

To date, all measurements and indirect determinations of nuclear parton distributions have been insensitive to the position of the interacting parton within the nucleus. However, there is no reason to expect the parton momentum distributions to be constant within the nucleus. They should at least vary with the local nuclear density. If shadowing is due to gluon recombination, the position dependence could be quite strong [4]. One way to probe the position dependence of the shadowing is to measure $c\overline{c}$ production over a wide range of impact parameters, thus scanning gluon localization in the nucleus. The charm quark production rate has been shown to be large in central collisions [5]; here, we will show that these studies are also feasible at large impact parameters.

This paper thus proposes a method for measuring the position dependence of the gluon momentum distribution in heavy nuclei. We show that the charm quark production rates in noncentral collisions are sensitive to the details of the gluon distribution and its position dependence. We use two different parametrizations of nuclear shadowing along with two parametrizations of the position dependence of the shadowing to calculate charm production in 100 GeV per nucleon Au+Au collisions at the Relativistic Heavy Ion Collider (RHIC) [6], now under construction at Brookhaven National Laboratory. However, the techniques discussed here should also be applicable to $c\overline{c}$ and $b\overline{b}$ production in Pb+Pb collisions at the CERN Large Hadron Collider (LHC). The charm quark production rate and p_T spectra are calculated as a function of the impact parameter b for noncentral collisions with impact parameters greater than the nuclear radius R_A.

For this study, we need to select events according to impact parameter. Although the impact parameter of the collision is not directly measurable, it may be inferred from the total transverse energy E_T of the event [7]. We discuss the relationship between E_T and b and present calculations showing that, for a given E_T, the impact parameter can be measured relatively accurately. Additional input, such as a measurement of nuclear breakup, through the use of a zero degree calorimeter, can refine this estimate.

Section II summarizes the calculations of $c\overline{c}$ production in peripheral collisions including a discussion of the nuclear parton shadowing and its possible spatial dependence. Section III discusses the relationship between transverse energy and impact parameter. Section IV presents the numerical results for the charm quark production rates and p_T spectra for two ranges of noncentral impact parameters. We demonstrate how these rates are sensitive to the nuclear gluon distribution. Our results are put into an experimental perspective in Sec. V. Finally, Sec. VI draws some conclusions.

II. $c\overline{c}$ PRODUCTION

To study the effects of shadowing on $c\overline{c}$ production in peripheral collisions, we emphasize the modifications of the parton distribution functions due to shadowing as well as the location of the interacting parton in the nucleus. We discuss the method used to calculate $c\overline{c}$ pair production and introduce two parametrizations of nuclear shadowing. We also describe two models of the spatial dependence of the shadowing.

The double differential cross section for $c\overline{c}$ pair production by nuclei A and B is

$$E_cE_{\bar c}\frac{d\sigma_{AB}}{d^3p_c d^3p_{\bar c}d^2b d^2r}=\sum_{i,j}\int dz dz' dx_1 dx_2 F_i^A(x_1,Q^2,\vec r,z)F_j^B(x_2,Q^2,\vec b-\vec r,z')E_cE_{\bar c}\frac{d\hat\sigma_{ij}(x_1P_1,x_2P_2,m_c,Q^2)}{d^3p_c d^3p_{\bar c}}. \tag{1}$$

Here i and j are the interacting partons in the nucleus and the functions F_i are the number densities of gluons, light quarks, and antiquarks evaluated at momentum fraction x, scale Q^2, and location $\vec r$, z. (Note that $\vec r$ is two dimensional.) The short-distance cross section $\hat\sigma_{ij}$ is calculable as a perturbation series in $\alpha_s(Q^2)$.

At leading order (LO), $c\bar c$ production proceeds by two basic processes

$$q+\bar q\to c+\bar c, \tag{2}$$

$$g+g\to c+\bar c. \tag{3}$$

The LO cross section to $\mathcal{O}(\alpha_s^2)$, can be written as

$$E_cE_{\bar c}\frac{d\sigma_{AB}}{d^3p_c d^3p_{\bar c}d^2b d^2r}=\int\frac{s}{2\pi}dz dz' dx_1 dx_2 C(x_1,x_2,Q^2,\vec r,z,\vec b-\vec r,z')\,\delta^4(x_1P_1+x_2P_2-p_c-p_{\bar c}), \tag{4}$$

where $\sqrt{s}$, the parton-parton center-of-mass energy, is related to $\sqrt{S}$, the hadron-hadron center-of-mass energy, by $s=x_1x_2S\geqslant 4m_c^2$, where the momentum fractions x_1 and x_2 are

$$x_{1,2}=\frac{m_T}{\sqrt{s}}(e^{\pm y}+e^{\pm\bar y}), \tag{5}$$

and $m_T=\sqrt{m_c^2+p_T^2}$. The target fraction x_2 decreases with rapidity while the projectile fraction x_1 increases. Here, the intrinsic transverse momenta of the incoming partons has been neglected. The convolution of the subprocess cross sections with the parton number densities is contained in $C(x_1,x_2,Q^2,\vec r,z,\vec b-\vec r,z')$ where

$$C(x_1,x_2,Q^2,\vec r,z,\vec b-\vec r,z')=\sum_q\,[F_q^A(x_1,Q^2,\vec r,z)F_{\bar q}^B(x_2,Q^2,\vec b-\vec r,z')+F_{\bar q}^A(x_1,Q^2,\vec r,z)F_q^B(x_2,Q^2,\vec b-\vec r,z')]\frac{d\hat\sigma_{q\bar q}}{dt}$$
$$+F_g^A(x_1,Q^2,\vec r,z)F_g^B(x_2,Q^2,\vec b-\vec r,z')\frac{d\hat\sigma_{gg}}{dt}. \tag{6}$$

Four-momentum conservation leads to the rather simple expression

$$\frac{d\sigma_{AB}}{dp_T^2dyd\bar y d^2bd^2r}=\int dz dz' x_1x_2C(x_1,x_2,Q^2,\vec r,z,\vec b-\vec r,z'). \tag{7}$$

The LO subprocess cross sections for $c\bar c$ production by $q\bar q$ annihilation and gg fusion, expressed as a function of m_T, y, and $\bar y$, are [9]

$$\frac{d\hat\sigma_{q\bar q}}{dt}=\frac{\pi\alpha_s^2}{9m_T^4}\frac{\cosh(y-\bar y)+m_c^2/m_T^2}{[1+\cosh(y-\bar y)]^3}, \tag{8}$$

$$\frac{d\hat\sigma_{gg}}{dt}=\frac{\pi\alpha_s^2}{96m_T^4}\frac{8\cosh(y-\bar y)-1}{[1+\cosh(y-\bar y)]^3}\times\left(\cosh(y-\bar y)+\frac{2m_c^2}{m_T^2}-\frac{2m_c^4}{m_T^4}\right). \tag{9}$$

Leading order calculations tend to underestimate the measured charm quark production cross section by a constant factor, usually called a K factor,

$$K_{\rm expt}^{\rm LO}=\frac{\sigma_{\rm expt}(AB\to c\bar c)}{\sigma_{\rm LO}(AB\to c\bar c)}. \tag{10}$$

The next-to-leading order (NLO) corrections to the LO cross section have been calculated [10,11] and an analogous theoretical K factor $K_{\rm th}$ can be defined from the ratio of the NLO to the LO cross sections,

$$K_{\rm th}=\frac{\sigma_{\rm NLO}(AB\rightarrow c\overline{c})}{\sigma_{\rm LO}(AB\rightarrow c\overline{c})}, \tag{11}$$

where $\sigma_{\rm NLO}$ is the sum of the LO cross section and the $\mathcal{O}(\alpha_s)$ corrections.

Previously [12], the NLO calculations were compared to the $c\overline{c}$ total production cross section data to fix m_c and Q so that $K^{\rm NLO}_{\rm expt}\sim 1$ to provide a more reliable estimate for nuclear collider energies. Reasonable agreement with the measured total cross section was found for $m_c=1.2$ GeV, $Q=2m_c$ for MRS D$-'$ the parton densities [13] and $m_c=1.3$ GeV, $Q=m_c$ for the parton densities GRV HO [14]. We choose different scales for the two sets[1] because of the different initial scales of the two parton distributions. The MRS D$-'$ distributions have $Q^2_{0,\rm MRS}=5$ GeV^2; we choose $Q=2m_c$ so that $Q^2>Q^2_{0,\rm MRS}$. The GRV HO sea quark and gluon distributions are valence-like at low x and $Q^2_{0,\rm GRV}=0.3$ GeV^2. We can then use $Q=m_c$ because $m_c^2>Q^2_{0,\rm GRV}$. However, below $Q^2\approx 5$ GeV^2 the gluon distribution is still somewhat valence-like.

When calculating inclusive distributions rather than total cross sections, it is more appropriate to choose $Q\propto m_T$, particularly when $p_T>m_c$ since a constant scale introduces unregulated collinear divergences [16]. Therefore, we take $Q=2m_T$ for the MRS D$-'$ distributions and $Q=m_T$ for the GRV HO distributions. Both sets of parton densities result in a NLO total $c\overline{c}$ production cross section of $\sim$350 μb in pp collisions at $\sqrt{S}=200$ GeV.

The differential $K_{\rm th}$ for the charm quark p_T distribution, the pair mass distribution, and the charm quark and $c\overline{c}$ pair rapidity distributions are nearly constant at RHIC energies [16]. They are also essentially independent of the parton density. The value of $K_{\rm th}$ is determined by a comparison of the NLO and LO total cross sections. Our LO calculations, Eq. (4), are multiplied by the appropriate $K_{\rm th}$ found for the specific parton density: 2.5 for the MRS D$-'$ distributions and 2.9 for the GRV HO distributions.

The nucleon parton densities are only a part of the space-dependent nuclear number densities $F_i^A(x,Q^2,\vec{r},z)$ introduced in Eq. (1). We have assumed that these nuclear number densities factorize into nuclear density distributions, independent of x and Q^2, the nucleon parton densities, independent of spatial position and A, and a shadowing function that parametrizes the modifications of the nucleon parton densities in the nucleus, dependent on x, Q^2, A, and location,

$$F_i^A(x,Q^2,\vec{r},z)=\rho_A(s)S^i(A,x,Q^2,\vec{r},z)f_i^p(x,Q^2),$$
$$F_i^B(x,Q^2,\vec{b}-\vec{r},z')=\rho_B(s')S^i(B,x,Q^2,\vec{b}-\vec{r},z')f_i^p(x,Q^2), \tag{12}$$

where $s=\sqrt{r^2+z^2}$, $s'=\sqrt{|\vec{b}-\vec{r}|^2+z'^2}$, and f_i^p are the nucleon parton densities. We assume that z and z' are uncorrelated. The collision geometry in the plane transverse to the beam is shown in Fig. 1.

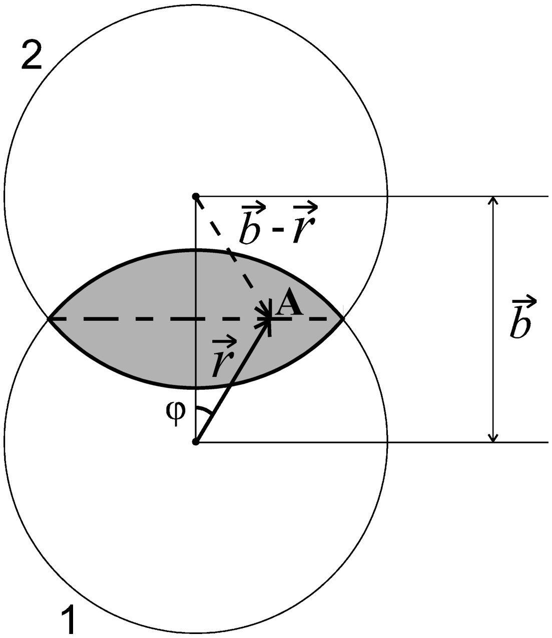

FIG. 1. The collision geometry of nuclear collisions in the plane transverse to the beam. The parton-parton collision point is indicated by A and b is the impact parameter.

A three-parameter Woods-Saxon shape is used to describe the nuclear density distribution,

$$\rho_A(s)=\rho_0\frac{1+\omega(s/R_A)^2}{1+\exp[(s-R_A)/d]}, \tag{13}$$

where R_A is the nuclear radius, d is the surface thickness, and ω allows for central irregularities. The electron scattering data of Ref. [17] is used for R_A, d, and ω assuming that the charge and matter density distributions are identical. The central density ρ_0 is found from the normalization $\int d^2r dz \rho_A(s)=A$. For gold, $\omega=0$, $d=0.535$ fm, $R_A=6.38$ fm, and $\rho_0=0.1693$ fm^{-3}.

If the parton densities in the nucleon and in the nucleus are the same, then $S^i(A,x,Q^2,\vec{r},z)\equiv 1$. We will use this as a baseline against which to compare our results with shadowing included.

We now discuss our choices of the shadowing parametrizations used in our calculations, independent of the position. Measurements of the nuclear charged parton distributions by deep-inelastic scattering on a nuclear target and a deuterium target show that the ratio $R_{F_2}=F_2^A/F_2^D$ has a characteristic shape as a function of x. The region below $x\sim 0.1$ is referred to as the shadowing region and the region $0.3<x<0.7$ is known as the EMC region. In both regions a depletion is observed in the heavy nucleus relative to deuterium and $R_{F_2}<1$. At very low x, $x\approx 0.001$, R_{F_2} appears to saturate[2] [19]. Between the shadowing and EMC regions, an enhance-

---

[1] These structure functions can be found in the CERN program library PDFLIB [15].

[2] We note that at even smaller values of x, shadowing within the nucleon itself is expected [4,18]. However, at RHIC energies, this very low x region is not expected to be reached.

ment, antishadowing, occurs where $R_{F_2} > 1$. There is also an enhancement as $x \to 1$, assumed to be due to Fermi motion of the nucleons. The general behavior of R_{F_2} as a function of x is often referred to as shadowing. Although this behavior is not well understood for all x, the shadowing effect can be modeled by an A-dependent fit to the nuclear deep-inelastic scattering data and implemented by a modification of the parton distributions in the proton. We use two different models of the relation between R_{F_2} and $S^i(A,x,Q^2)$. These two parametrizations were used earlier to estimate the effect of shadowing on $c\overline{c}$ and $b\overline{b}$ production in central collisions [5] with no spatial dependence assumed for the shadowing.

The first parametrization is a fit to recent nuclear deep-inelastic scattering data. The fit does not differentiate between quark, antiquark, and gluon modifications and does not include evolution in Q^2. Therefore it is not designed to conserve baryon number or momentum. We define $R_{F_2} = S_1(A,x)$ [20] with

$$S_1(A,x) = \begin{cases} R_s \dfrac{1 + 0.0134(1/x - 1/x_{\rm sh})}{1 + 0.0127A^{0.1}(1/x - 1/x_{\rm sh})}\,, & x < x_{\rm sh}\,, \\ a_{\rm EMC} - b_{\rm EMC}x, & x_{\rm sh} < x < x_{\rm Fermi}\,, \\ R_f \left(\dfrac{1 - x_{\rm Fermi}}{1 - x} \right)^{0.321}, & x_{\rm Fermi} < x < 1, \end{cases} \tag{14}$$

where $R_s = a_{\rm EMC} - b_{\rm EMC} x_{\rm sh}$, $R_f = a_{\rm EMC} - b_{\rm EMC} x_{\rm Fermi}$, $b_{\rm EMC} = 0.525(1 - A^{-1/3} - 1.145A^{-2/3} + 0.93A^{-1} + 0.88A^{-4/3} - 0.59A^{-5/3})$, and $a_{\rm EMC} = 1 + b_{\rm EMC} x_{\rm EMC}$. The fit fixes $x_{\rm sh} = 0.15$, $x_{\rm EMC} = 0.275$, and $x_{\rm Fermi} = 0.742$. Thus, the nuclear parton densities are modified so that

$$f_i^A(x,Q^2) = S_1(A,x) f_i^p(x,Q^2). \tag{15}$$

The second parametrization $S_2^i(A,x,Q^2)$ modifies the valence and sea quark and gluon distributions separately and also includes Q^2 evolution [21], but is based on an older fit to the data using the Duke-Owens parton densities [22]. The initial scale for the evolution is $Q_0 = 2$ GeV and the Q^2 evolution is studied with both the standard Altarelli-Parisi evolution and with modifications due to gluon recombination at high density. The gluon recombination terms do not strongly alter the evolution. In this case, the nuclear parton densities are modified so that

$$f_V^A(x,Q^2) = S_2^V(A,x,Q^2) f_V^p(x,Q^2), \tag{16}$$

$$f_S^A(x,Q^2) = S_2^S(A,x,Q^2) f_S^p(x,Q^2), \tag{17}$$

$$f_G^A(x,Q^2) = S_2^G(A,x,Q^2) f_G^p(x,Q^2), \tag{18}$$

where $f_V = u_V + d_V$ is the valence quark density and $f_S = 2(\overline{u} + \overline{d} + \overline{s})$ is the total sea quark density. We assume that S_2^V and S_2^S affect the up, down, and strange valence and sea quarks identically. The ratios were constrained by assuming that $R_{F_2} \approx S_2^V$ at large x and $R_{F_2} \approx S_2^S$ at small x since $x f_V^p(x,Q_0^2) \to 0$ as $x \to 0$. For the gluons, we take $R_{F_2} \approx S_2^G$ for all x [21], since one might expect more shadowing for the sea quarks, generated from gluons, at small x. These parton densities do conserve baryon number, $\int_0^1 dx f_V^{p,A}(x,Q^2) = 3$, and momentum, $\int_0^1 dx x[f_V^{p,A}(x,Q^2) + f_S^{p,A}(x,Q^2) + f_G^{p,A}(x,Q^2)] = 1$, at all Q^2. We have used the MRS D$-'$ and GRV HO densities with S_2^i instead of the Duke-Owens densities, leading to some small deviations in the momentum sum but the general trend is unchanged.

Since the shadowing is likely related to the nuclear density, it should also depend on the spatial distribution of the partons within the nucleus so that $S^i(A,x,Q^2,\vec{r},z) \to 1$ as $s \to \infty$. The reduced shadowing is reasonable since the shadowing mechanism should be less effective when the nuclear density is low. This spatial dependence should also be normalized so that $(1/A)\int d^2r dz \rho(s) S^i(A,x,Q^2,\vec{r},z) = S^i(A,x,Q^2)$ to recover the deep-inelastic scattering results which do not have any explicit impact parameter dependence. This approach may fail when $x \to 1$, because then the change in the structure function is likely due to Fermi motion, which should not exhibit spatial dependence.

One natural parametrization of the spatial dependence follows the nuclear matter density distribution,

$$\begin{aligned} S^i_{\rm WS} = S^i(A,x,Q^2,\vec{r},z) &= 1 + N_{\rm WS} \frac{S^i(A,x,Q^2) - 1}{1 + \exp[(s - R_A)/d]} \\ &= 1 + N_{\rm WS}[S^i(A,x,Q^2) - 1] \frac{\rho(s)}{\rho_0}\,, \end{aligned} \tag{19}$$

where $N_{\rm WS} = 1.317$ is needed for the normalization to $S^i(A,x,Q^2)$. This form of the spatial dependence has a rather weak dependence on s until the nuclear surface is approached. Note that when $s \to 0$, $S^i_{\rm WS} < S^i$ in the shadowing and EMC regions while $S^i_{\rm WS} > S^i$ in the antishadowing region.

The actual spatial dependence of shadowing may be stronger if the shadowing effect is not directly related to the nuclear matter density distribution. This can occur if the gluons are not well localized within the nucleus. One can alternatively assume that the shadowing is related to the nuclear thickness at the collision point, proportional to the distance a parton from one nucleus travels through the other [23]. Therefore we also consider

$$S^i_{\mathrm{R}}(A,x,Q^2,\vec{r},z)=\begin{cases}1+N_{\mathrm{R}}[S^i(A,x,Q^2)-1]\sqrt{1-(r/R_A)^2} & r\leq R_A\\ 1 & r>R_A,\end{cases} \tag{20}$$

where $N_{\mathrm{R}}=1.449$ assures the normalization after the average over $\rho(s)$. Similarly, when $s\to 0$, $S^i_{\mathrm{R}}<S^i$ in the shadowing and EMC regions while $S^i_{\mathrm{R}}>S^i$ in the antishadowing region. The normalization is higher here because of the larger region over which the suppression due to shadowing is reduced relative to S^i_{WS}.

We calculate the $c\overline{c}$ production cross sections in peripheral nuclear collisions with $S^i(A,x,Q^2)=1$, S_1, and S^i_2. As we will show, the shape of the inclusive charm quark p_T distributions are similar for S_1 and S^i_2. Therefore, we model the spatial dependence of S_1 only, according to Eqs. (19) and (20).

III. CORRELATION BETWEEN E_T AND IMPACT PARAMETER

Although the impact parameter is not directly measurable, it can be related to direct observables. We discuss here the indirect measurement of the impact parameter b by means of the transverse energy E_T [7,24]. Here $E_T=\Sigma_i\sqrt{m_i^2+p_{Ti}^2}$, summed over all detected particles in the event with masses m_i and transverse momenta p_{Ti}. It is also possible to infer the impact parameter by a measurement of the nuclear breakup since the beam remnants deposited in a zero degree calorimeter are correlated with the impact parameter. A measure of the total charged particle multiplicity, proportional to E_T, could be used to refine the impact parameter determination.

The transverse energy contains "soft" and "hard" components. The "hard" components arise from quark and gluon interactions above momentum p_0, the scale above which perturbative QCD is assumed to be valid. Minijet production, calculated for $p_{T,\mathrm{jet}}>p_0\sim 2$ GeV [25], becomes an important contribution to the dynamics of the system in high-energy nucleus-nucleus collisions. The hard cross section $\sigma_H^{pp}(p_0)=2\sigma_{\mathrm{jet}}$, twice the single LO minijet production cross section, can be calculated perturbatively. "Soft" processes with $p_T<p_0$ are not perturbatively calculable, yet they produce a substantial fraction of the measured E_T at high energies (and almost the entire E_T at CERN SPS energies). These processes must be modeled phenomenologically. We assume $\sigma_S^{pp}=\sigma_{\mathrm{inelastic}}^{pp}$, the inelastic pp scattering cross section. Our calculation of the total E_T distribution follows Ref. [24].

If the hard component is formed by independent parton-parton collisions, then the average number of hard parton-parton collisions as a function of b, $N^H_{AA}(b)$, is

$$\overline{N^H_{AA}}(b)=T_{AA}(b)\sigma_H^{pp}(p_0), \tag{21}$$

where $\sigma_H^{pp}(p_0)\sim 6.5$ mb at RHIC [25] and $T_{AA}(b)$ is the nuclear overlap function,

$$T_{AA}(b)=\int d^2r\,T_A(\vec{r})T_A(\vec{b}-\vec{r}), \tag{22}$$

where the nuclear thickness function is defined as $T_A(\vec{r})=\int dz\,\rho_A(z,\vec{r})$. In Au+Au collisions at $b=0$, $T_{AA}=29/\mathrm{mb}$ [26]. The E_T distribution can be expressed as [24]

$$\frac{d\sigma_H}{dE_T}=\int d^2b\,\Sigma_{N=1}^{\infty}\frac{[\overline{N^H_{AA}}(b)]^N}{N!}\exp[-\overline{N^H_{AA}}(b)]\times\int\prod_{i=1}^{N}dE_{Ti}\frac{1}{\sigma_H^{pp}}\frac{d\sigma_H^{pp}}{dE_{Ti}}\delta(E_T-\Sigma_{i=1}^{N}E_{Ti}). \tag{23}$$

If $\overline{N^H_{AA}}$ is large, $d\sigma_H/dE_T$ can be approximated by the Gaussian [24]

$$\frac{d\sigma_H}{dE_T}=\int d^2b\frac{1}{\sqrt{2\pi\sigma_H^2(b)}}\exp\left(-\frac{[E_T-\overline{E^{AA}_{TH}}(b)]^2}{2\sigma_H^2(b)}\right), \tag{24}$$

where the mean E_T, $\overline{E^{AA}_{TH}}(b)$, and standard deviation, $\sigma_H(b)$, are proportional to the first and second E_T moments of the hard cross section,

$$\overline{E^{AA}_{TH}}(b)=T_{AA}(b)\sigma_H^{pp}(p_0)\langle E_T\rangle_H^{pp}, \tag{25}$$

$$\sigma_H^2(b)=T_{AA}(b)\sigma_H^{pp}(p_0)\langle E_T^2\rangle_H^{pp}. \tag{26}$$

In the rapidity interval $|y|\leq 0.5$, $\sigma_H^{pp}(p_0)\langle E_T\rangle_H^{pp}\approx 17$ mb GeV and $\sigma_H^{pp}(p_0)\langle E_T^2\rangle_H^{pp}\approx 70$ mb GeV^2 [25].

At RHIC energies, the hard part does not dominate the soft component, proportional to the number of nucleon-nucleon collisions,

$$\overline{N^S_{AA}}(b)=T_{AA}(b)\sigma_S^{pp}, \tag{27}$$

where $\sigma_S^{pp}\sim 30$ mb. Since the soft component is almost independent of the collision energy, we assume, as in Ref. [24], that the hard and soft components are separable on the pp level and thus independent of each other at fixed b. Therefore the total E_T distribution is a convolution of the hard and soft components with total mean and standard deviation,

$$\overline{E^{AA}_{T}}(b)=T_{AA}(b)[\sigma_H^{pp}(p_0)\langle E_T\rangle_H^{pp}+\epsilon_0], \tag{28}$$

$$\sigma^2(b)=T_{AA}(b)[\sigma_H^{pp}(p_0)\langle E_T^2\rangle_H^{pp}+\epsilon_1], \tag{29}$$

where ϵ_0 and ϵ_1 are taken from lower-energy data and adjusted to the same rapidity interval as the hard component, $|y|\leq 0.5$, $\epsilon_0=15$ mb GeV, $\epsilon_1=50$ mb GeV^2 [24]. Shadowing, which affects the hard component by reducing the minijet cross section, is not included in these averages. Multiply-

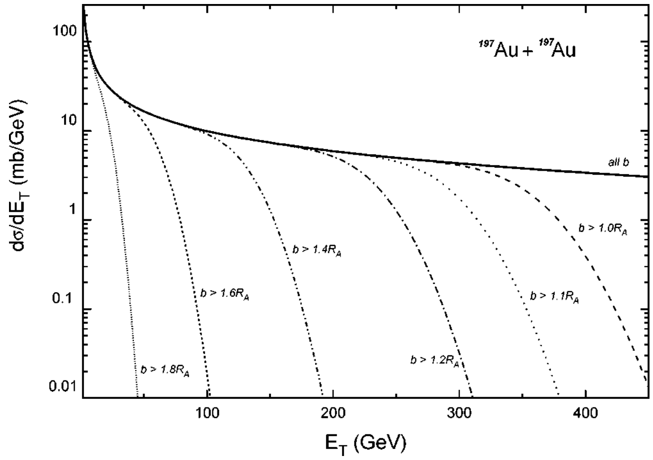

FIG. 2. Cross section as a function of E_T, for a selection of impact parameters ranges.

ing σ_H^{pp} by a shadowing factor modifies the E_T distribution by less than 10% [27]. A correction has been included here.

Figure 2 shows the E_T distribution (for $y<|0.5|$) for 100 GeV/nucleon Au+Au collisions for several different impact parameter intervals as well as the total cross section. Singling out a particular E_T range can therefore select a rather narrow distribution of impact parameters. For example, requiring $E_T<300$ GeV selects almost exclusively events with $b>R_A$ while $E_T<180$ GeV selects events with $b>1.2R_A$.

Good event purity can be obtained with even narrower selections. For example, 300 GeV $>E_T>180$ GeV largely corresponds to $1.2R_A>b>R_A$. An example of the purity can be seen in Fig. 3 which shows the range of impact parameters at $E_T=200$ GeV. The distribution is centered at $b=1.27R_A$ with a standard deviation $\sigma\sim 0.05R_A$. Approximately 90% of the events fall into the range $1.15R_A<b<1.35R_A$, narrow enough to be an effective impact parameter selector. Thus at $E_T=200$ GeV, the impact parameter can be measured to within 10%. However, the statistical accuracy depends on the average number of collisions, proportional to E_T, so that $\sigma/b\approx 1/\sqrt{E_T}$.

For very small E_T, complications arise. The first concerns the transition from Eq. (23) to Eq. (24) which is only valid if $\overline{N_{AA}^H}(b)$ is large enough for the Poisson distribution to be approximated by a Gaussian. For a small number of collisions, Eq. (24) overestimates the number of low E_T events, even allowing a finite probability for negative E_T events. In practice, the agreement is quite good even at $b=1.8R_A$, corresponding to $T_{AA}=0.9$/mb, $N_{AA}^H=5.5$, and $E_T\approx 30$ GeV. At significantly smaller E_T a correction is needed. Further, the event-by-event fluctuations are large when the collision number is small, increasing the uncertainty in the impact parameter measurement.

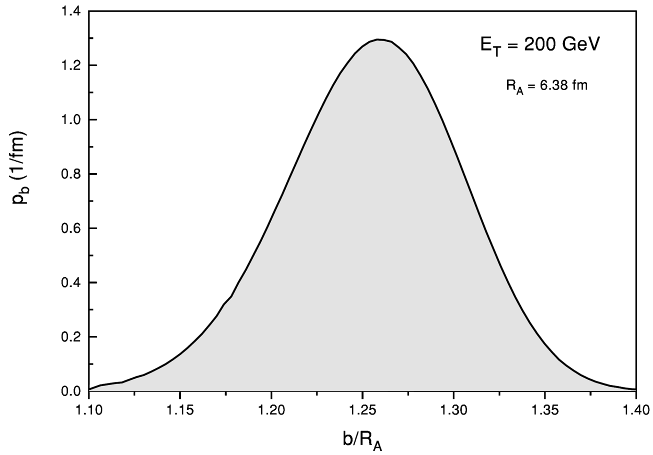

FIG. 3. Distribution of impact parameter for events with $E_T=200$ GeV.

At small E_T the presence of charmed quarks will alter the relationship between E_T and impact parameter because a $c\overline{c}\to D\overline{D}$ pair must have $E_T>2m_D\approx 3.7$ GeV. Typical values are $E_T\sim 4-6$ GeV. Thus, when $E_T<20$ GeV, the relationship between E_T and b in charm events will be different. This altered relationship can be studied in simulations to correct the data.

Finally, other types of interactions can contribute to charm quark production at low E_T. The largest identified charm quark contribution in very peripheral collisions is photon-gluon fusion [8,28].

Any real detector can only measure E_T in a limited rapidity interval. For example, the calorimeter of the STAR detector at RHIC will cover the range $-1<y<2$ [29]. The acceptance can be compensated by appropriately modifying $\langle E_T\rangle_H^{pp}$, $\langle E_T^2\rangle_H^{pp}$, ϵ_0, and ϵ_1, given here for $|y|<0.5$. The accuracy scales roughly as the square root of the observed energy. A large acceptance can also extend the region of validity of Eq. (24) to larger b.

The major source of systematic uncertainty here lies in the scaling, division into hard and soft components, and in accurately calculating the hard cross section at high energies. The spatial dependence of shadowing, discussed in the following section, will also contribute uncertainty to the impact parameter measurement. However, this uncertainty should be less than the 10% change due to the inclusion of shadowing [27]. These uncertainties can be investigated by comparing the measured $d\sigma/dE_T$ curve to the geometric $d\sigma/db$ at small impact parameters. We expect that, for $b>1.2R_A$, the systematic errors will be comparable to the statistical.

The noncentral event selection technique to constrain the impact parameter may be useful in other analyses of heavy ion data. At large impact parameters, only the outer portions of the nuclei are involved, but as the collision centrality increases, the nuclear interior is more deeply probed. Therefore the impact parameter variation roughly corresponds to the portion of the nucleus involved in the interaction, and can thus be used to study the difference between the parton constituents of the nuclear core and those near the surface.

IV. RESULTS

The best way to determine the gluon momentum fraction is to detect both charm quarks. Then x_1 and x_2 can be fixed exactly and the shadowing mapped out. The measurements are relatively easy to interpret if $y=-\overline{y}$ since $x_1=x_2$. After first discussing the general results when the kinematic variables are integrated over, we show the p_T distributions for the MRS D$-'$ and GRV HO parton densities assuming both the c and $\overline{c}$ are detected. The low experimental efficiency for detecting charm suggests that it is unlikely for both

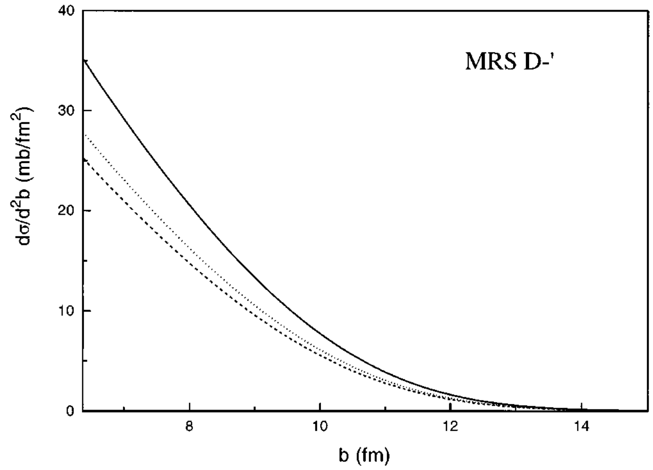

FIG. 4. Charm production cross section as a function of b for the MRS D$-'$ parton densities, with $S=1$ (solid line) and with two nuclear shadowing parametrizations S_1 (dashed line) and S_2 (dotted line).

quarks to be detected in an event. Thus we subsequently discuss the feasibility of the study if only one of the charm quarks is detected.

Figure 4 shows the $c\overline{c}$ production cross section as a function of impact parameter for $b>R_A$ with $S=1$, S_1, and S_2 at RHIC [6]. The cross sections were calculated by integrating Eq. (1) over the c and $\overline{c}$ four-momenta. The rates for these noncentral collisions are still quite large. Without shadowing, for $b>1.2R_A$ the charm cross section is 2.9 b while for $b>1.8R_A$ it is still 200 mb. At the RHIC Au+Au design luminosity, 2×10^{26} cm^{-2} sec^{-1} [6], this results in 6300 and 430×10^{6} $c\overline{c}$ pairs/year (3000 h). Thus these measurements will not be statistics limited, even with the roughly 35% reduction in cross section when shadowing is included.

Figures 5 and 6 show the charm quark p_T distributions in two different impact parameter intervals, $b>1.2R_A$, roughly corresponding to $E_T<180$ GeV in Fig. 2, and $b>1.8R_A$, for several selected c and $\overline{c}$ quark rapidities. The results with the MRS D$-'$ and GRV HO parton densities are compared. By measuring charm quarks as a function of p_T for a variety of rapidities, different values of x_1 and x_2 are probed. For example, $p_T=0$, $y=\overline{y}=0$ corresponds to $x_1=x_2=1.3\times10^{-2}$ while $p_T=0$, $y=2$, and $\overline{y}=-2$ corresponds to $x_1=x_2=5.1\times10^{-2}$. At $p_T\approx2.1$ GeV, x_1 and x_2 are doubled, moving into the antishadowing region for $|y|=2$. Thus varying x_1 and x_2 changes the relative strength of the shadowing. Calculations with $S=1$, S_1, $S_{1,\mathrm{WS}}$, $S_{1,\mathrm{R}}$, and S_2 are shown in each case.

In every case considered, the unshadowed cross section is larger than the shadowed cross sections. The total $c\overline{c}$ production cross sections with $Q\propto nm_c$ differ only by 2% in pp collisions. (Recall that $n=2$ for MRSD$-'$ and $n=1$ for GRV HO.) When the total cross section is computed by integrating an inclusive cross section where $Q\propto nm_T$, the difference increases to $\approx6\%$ due to the running scale in the parton distributions and α_s. The inclusive distributions reflect the low x and Q^2 behavior of the parton distributions. The MRS D$-'$ gluon distributions are always decreasing as a function of p_T. However, the GRV HO gluon distributions are still valence-like at low Q. Thus for $y=\overline{y}=0$ and $p_T<1.5$ GeV the gluon distribution continues to increase, causing the observed $\approx15\%$ difference between the $S=1$ distributions at $p_T\approx0$ in Figs. 5(a) and 5(d). At larger rapidity and x, such as in Figs. 5(c) and 5(f), the difference is reduced to $\approx8\%$.

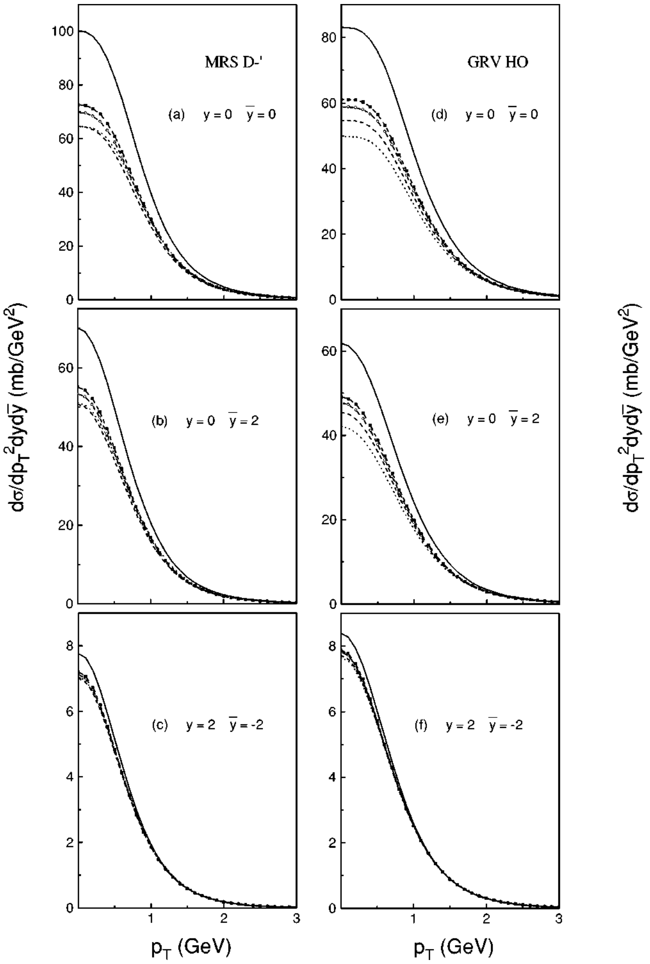

FIG. 5. The p_T distribution of $c\overline{c}$ pairs for the MRS D$-'$ (a), (b), and (c) and GRV HO (d), (e), and (f) parton densities. We have selected events with $b>1.2R_A$ and three values of the c and $\overline{c}$ quark rapidities: $y=0$, $\overline{y}=0$ in (a) and (d); $y=0$, $\overline{y}=2$ in (b) and (e); $y=2$, $\overline{y}=-2$ in (c) and (f). The solid curves are with $S=1$. The spatially independent shadowing results are given in the dashed and dotted curves for S_1 and S_2, respectively. The effect of the spatial dependence on S_1 is also shown. The dashed curve with the solid squares shows the result with $S_{1,\mathrm{R}}$ and the dashed curve with the open circles gives the result with $S_{1,\mathrm{WS}}$. In (a), (b), (d), and (e) the S_1 and $S_{1,\mathrm{WS}}$ curves overlap.

The shadowing functions affect the charm p_T distributions differently for the MRS D$-'$ and GRV HO parton distributions because of the difference in the scale Q^2. In general S_2^G increases more rapidly with x than S_1 between the shadowing and antishadowing regions. With the MRS D$-'$ parton distributions, at $p_T\approx0$, $S_1\approx S_2^G$ for $Q\approx2m_c$. As p_T increases, $S_2^G>S_1$ due to the evolution of S_2. Therefore, when $p_T\approx1$ GeV, the p_T distribution with S_2 will be $\approx10\%$ larger than the distribution with S_1. This continues to hold as p_T rises, as shown in Figs. 5(a), 5(b), and 5(c). The GRV HO case is different because of the lower scale. There, the evo-

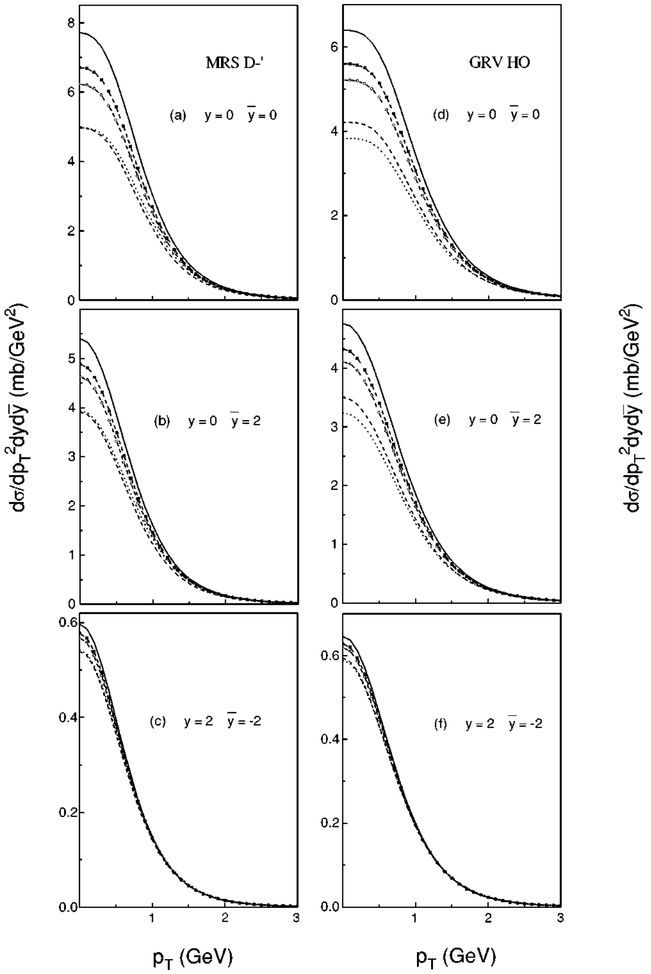

FIG. 6. The same as in Fig. 5 but with $b > 1.8R_A$.

lution of S_2 with Q^2 does not begin until $Q_0 = 2$ GeV, corresponding to $p_T \approx 1.5$ GeV. For $p_T < 1.5$ GeV, $S_1 > S_2^G$. At $p_T \approx 2$ GeV for $y = \overline{y} = 0$, the evolution of S_2^G causes the situation to be reversed and $S_2^G > S_1$, as can be seen by inspection of Fig. 5(d). At larger rapidities, the larger slope of S_2^G in the shadowing region cause the switch between S_1 and S_2 dominance to occur at lower values of p_T, even before the evolution of S_2^G begins, since x is larger at small p_T and large y.

Including spatial dependence in S_1 increases the cross section toward the $S = 1$ value at high b where the nuclear density is low. The cross section is now larger because the lower density near the nuclear surface reduces the shadowing. As the impact parameter rises, the tails of the density distributions are probed and the shadowed cross sections approach the $S = 1$ result. This happens relatively slowly, especially for $S_{1,\mathrm{WS}}$, since the density is nearly constant except within d of the surface. The shadowing is thus almost constant except near the nuclear surface. For gold, $d = 0.535$ fm while $b = 1.8R_A$, the lower bound on the impact parameter in Fig. 6, corresponds to collisions within 1.2 fm of the surface so that some collisions occur below the surface layer in at least one nucleus. In both Figs. 5 and 6, $S_{1,\mathrm{R}} > S_{1,\mathrm{WS}}$ because the dependence on the nuclear thickness (albeit for a spherical nucleus) decreases the effects of shadowing already at small r while $S_{1,\mathrm{WS}}$ is almost constant. The effect is more apparent for larger impact parameters. When $b > 1.2R_A$, both spatial forms increase the cross section about 15% over S_1. For $b > 2R_A$ the spatial results are approximately halfway between the cross sections with $S = 1$ and $S = S_1$. The similarity of results between the two spatial parametrizations suggests that the parton localization measurements may not be too hard to interpret.

Thus measurements of charm quark production at large impact parameters probe the nuclear surface where shadowing effects are greatly reduced, and, for extremely peripheral collisions, the limit of independent pp collisions is regained. As the collisions become more central, the charm quark production rate should begin to deviate from the naive expectation from superimposed pp collisions. By measuring charm production as a function of impact parameter, it is possible to watch the shadowing turn on with the rate of increase providing a measure of parton localization in the nucleus.

So far we have assumed that both the c and $\overline{c}$ quarks are detected. Given the low efficiency for detecting charm quarks, either by their semileptonic decays or by reconstruction of specific final states, it is worth considering what can be learned if only one of the quarks is detected. Figure 7 shows the rapidity distribution of the $\overline{c}$ quark, assuming that the c quark is detected at $y = 0$ and $p_T = 0$ assuming $S = 1$, S_1, S_2, $S_{1,\mathrm{WS}}$, and $S_{1,\mathrm{R}}$. Kinematically, this situation corresponds to charm pair invariant mass $M^2 = 2m_c^2(1 + \cosh \overline{y})$ so that increasing $\overline{y}$ corresponds to increasing phase space along with increasing invariant mass. The cross section increases until $y \approx \pm 1$ where $M \approx 3.4$ GeV and decreases with larger M, typical for invariant mass distributions [12]. Figure 8 shows the single charm p_T distribution at $y = 0$ integrated over $\overline{y}$ for $b > 1.8R_A$. The results are similar to the case when both quarks are detected. Although some information is lost if only a single quark is detected, the trends remain the same as those seen in Fig. 6. Therefore it should still be possible to extract the shadowing information from the data.

V. DISCUSSION

If the charmed quark rapidity and momentum can be measured over a broad range of impact parameters, the gluon momentum distribution and its spatial/density dependence can be measured. However, there are a number of difficulties involved in relating these calculations to measurements. Charm is normally detected either via its semileptonic decays or through reconstruction of selected decay modes. While the detection of leptons from semileptonic decays is fairly straightforward, the lepton p_T and y differ from that of the parent hadron. The parent hadron distribution can also differ slightly from that of the initially produced quark although the hadronic environment reduces this effect [30]. While this momentum shift does not create any fundamental problems, it adds another intermediate step which must be correctly modeled. Fully reconstructed charm decays such as $D^{*+} \rightarrow D^0 \pi^+ \rightarrow (K^- \pi^+) \pi^+$ could allow for a full reconstruction of the meson direction, reducing the uncertainty in the determination of the charmed quark p_T and y. However, the small branching ratios and low efficiency for detecting these decays probably preclude the useful detection of both charmed quarks in a pair.

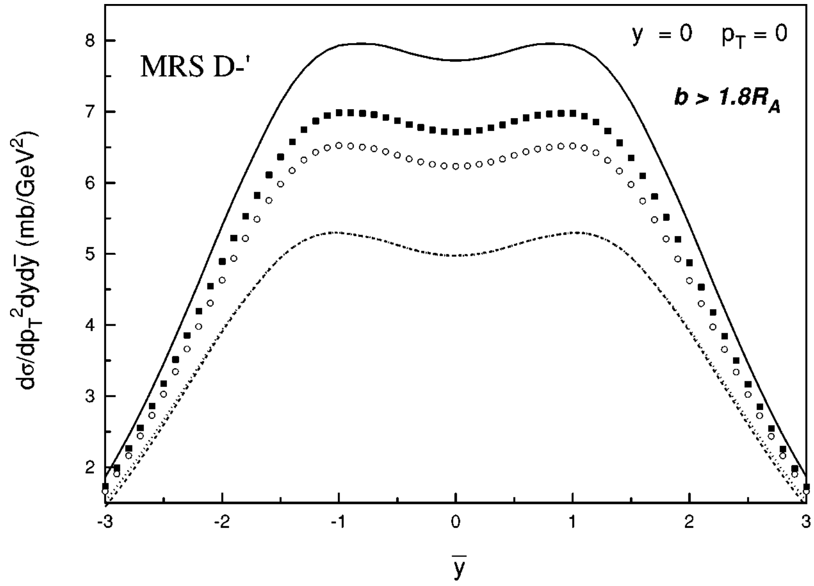

FIG. 7. The $\bar{c}$ rapidity distribution for $p_T=0$ and the charm quark is produced at $y=0$. The solid curve is with $S=1$. The spatially independent shadowing results are given in the dashed and dotted curves for S_1 and S_2, respectively. The effect of the spatial dependence on S_1 is also shown. The solid squares show the result with $S_{1,\mathrm{R}}$ and the open circles give the result with $S_{1,\mathrm{WS}}$.

In addition to gold, RHIC will accelerate a variety of lighter nuclei. The surface layer is a larger fraction of the nuclear radius in lighter nuclei. In this case, the Woods-Saxon and square root spatial dependences should more closely match over the full range of impact parameters. Since RHIC is also a pA collider, the gluon localization could in principle be probed for an individual nucleus. However, for pA, the number of collisions is small enough for the Gaussian approximation to break down, rendering the E_T to b correlation problematic. For pA, a useful relationship between E_T and b has not been demonstrated. However, if the impact parameter could be determined, the techniques discussed here could be used to study shadowing. One of the nuclear structure functions would merely be replaced with that for a free proton. The A dependence of charm production at various impact parameters can in any case provide an additional handle on interplay between shadowing and its spatial dependence. For pA, dileptons can also be used to probe gluon shadowing [31].

At LHC, similar calculations can be made for $c\bar{c}$ and $b\bar{b}$ production. The higher energy implies that the charm and bottom pairs will be produced at much lower x, increasing

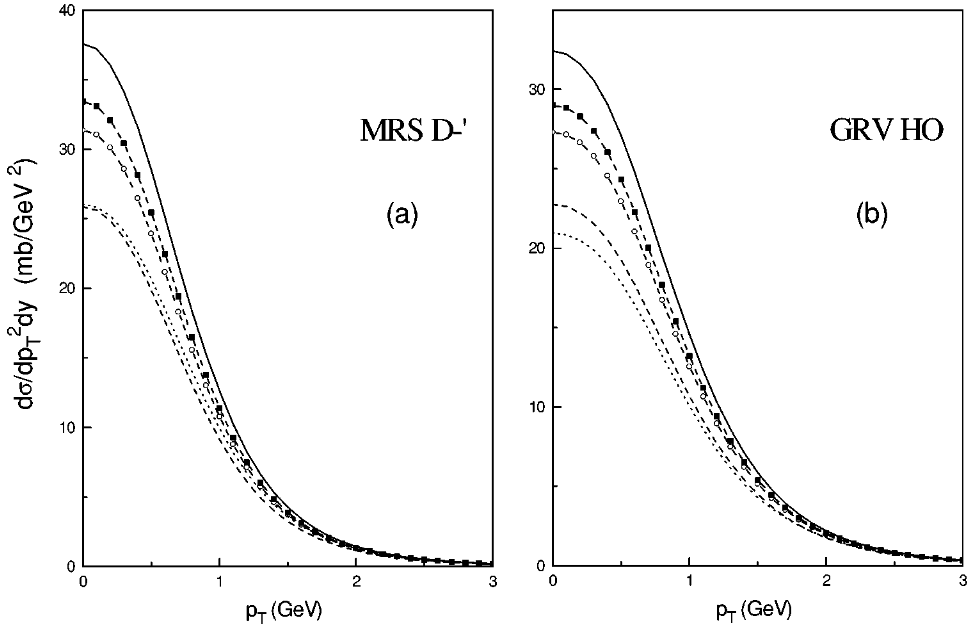

FIG. 8. The p_T distribution for single charm quarks with $y=0$ for MRS D$-'$ (a) and GRV HO (b) parton densities. We have selected events with $b>1.8R_A$. The solid curves are with $S=1$. The spatially independent shadowing results are given in the dashed and dotted curves for S_1 and S_2, respectively. The effect of the spatial dependence on S_1 is also shown. The dashed curve with the solid squares shows the result with $S_{1,\mathrm{R}}$ and the dashed curve with the open circles gives the result with $S_{1,\mathrm{WS}}$.

the importance of shadowing and further reducing the production cross sections. Thus the sensitivity of the cross section to the spatial dependence will be enhanced.

VI. CONCLUSIONS

We have calculated charmed quark production in noncentral Au+Au collisions for several different structure functions and assumptions about nuclear shadowing.

Shadowing reduces the charm production cross section up to 35%. However, when the spatial dependence of shadowing is included, the effect is decreased. By measuring the charmed quark production rates as a function of impact parameter, it is possible to study the effect of shadowing and to detect, for the first time, its localization within the nucleus. This spatial dependence provides an indication of the gluon recombination distance scale.

The correlation between impact parameter and transverse energy has been used to fix b. We have shown that the impact parameter determination is reliable to within a 10% statistical uncertainty on an event-by-event basis for $b \approx 1.2R_A$. The systematic errors are expected to be comparable.

ACKNOWLEDGMENTS

V.E. and A.K. would like to thank the LBNL Relativistic Nuclear Collisions group for their hospitality and M. Strikhanov for discussions and support. We also thank K. J. Eskola for providing the shadowing routines and for discussions. This work was supported in part by the Director, Office of Energy Research, Division of Nuclear Physics of the Office of High Energy and Nuclear Physics of the U.S. Department of Energy under Contract No. DE-AC03-76SF0098.

[1] J. J. Aubert *et al.*, Nucl. Phys. **B293**, 740 (1987); M. Arneodo, Phys. Rep. **240**, 301 (1994).

[2] D. M. Alde *et al.*, Phys. Rev. Lett. **66**, 133 (1991).

[3] J. J. Appel, Annu. Rev. Nucl. Part. Sci. **42**, 367 (1992).

[4] L. V. Gribov, E. M. Levin, and M. G. Ryskin, Phys. Rep. **100**, 1 (1983).

[5] S. Gavin, P. L. McGaughey, P. V. Ruuskanen, and R. Vogt, Phys. Rev. C **54**, 2606 (1996).

[6] ‘‘Conceptual Design for the Relativistic Heavy Ion Collider,’’ Brookhaven National Laboratory Report No. BNL-52195, 1989.

[7] V. Emel’yanov, A. Khodinov, and M. Strikhanov, Yad. Fiz. **60**, 465 (1997) [Phys. At. Nucl. **60**, 539 (1997)].

[8] M. Greiner *et al.*, Phys. Rev. C **51**, 911 (1995).

[9] R. K. Ellis, in ‘‘Physics at the 100 GeV Scale,’’ Proceedings of the 17th SLAC Summer Institute, Stanford, California, 1989, edited by E. C. Brennan, SLAC Report No. 361, Stanford, 1990.

[10] P. Nason, S. Dawson, and R. K. Ellis, Nucl. Phys. **B303**, 607 (1988); **B327**, 49 (1989).

[11] W. Beenakker, H. Kuijf, W. L. van Neerven, and J. Smith, Phys. Rev. D **40**, 54 (1989); W. Beenakker, W. L. van Neerven, R. Meng, G. A. Schuler, and J. Smith, Nucl. Phys. **B351**, 507 (1991).

[12] P. L. McGaughey *et al.*, Int. J. Mod. Phys. A **10**, 2999 (1995).

[13] A. D. Martin, W. J. Stirling, and R. G. Roberts, Phys. Lett. B **306**, 145 (1993).

[14] M. Glück, E. Reya, and A. Vogt, Z. Phys. C **53**, 127 (1992).

[15] H. Plothow-Besch, Comput. Phys. Commun. **75**, 396 (1993).

[16] R. Vogt, Z. Phys. C **71**, 475 (1996).

[17] C. W. deJager, H. deVries, and C. deVries, At. Data Nucl. Data Tables **14**, 485 (1974).

[18] L. V. Gribov, E. M. Levin, and M. G. Ryskin, Nucl. Phys. **B188**, 555 (1981); Zh. Eksp. Teor. Fiz. **80**, 2132 (1981) [Sov. Phys. JETP **53**, 1113 (1981)]; A. H. Mueller and J. W. Qiu, Nucl. Phys. **B258**, 427 (1986).

[19] M. R. Adams *et al.*, Phys. Rev. Lett. **68**, 3266 (1992).

[20] K. J. Eskola, J. Qiu, and J. Czyzewski (private communication).

[21] K. J. Eskola, Nucl. Phys. **B400**, 240 (1993).

[22] D. W. Duke and J. F. Owens, Phys. Rev. D **30**, 49 (1984).

[23] X.-N. Wang and M. Gyulassy, Phys. Rev. D **44**, 3501 (1995).

[24] K. J. Eskola, K. Kajantie, and J. Lindfors, Nucl. Phys. **B323**, 37 (1989).

[25] K. J. Eskola, Nucl. Phys. **A590**, 383 (1995); K. J. Eskola, K. Kajantie, and P. V. Ruuskanen, Phys. Lett. B **332**, 191 (1994).

[26] K. J. Eskola, R. Vogt, and X.-N. Wang, Int. J. Mod. Phys. A **10**, 3087 (1995).

[27] K. J. Eskola, Z. Phys. C **51**, 633 (1991).

[28] V. Emel’yanov, A. Khodinov, and M. Strikhanov, Report No. MEPHI-026, 1995.

[29] W. B. Christie, in ‘‘Physics with the Collider Detectors at RHIC and the LHC,’’ edited by J. Thomas and T. J. Hallman, Report No. UCRL-ID-121571, 1995 (unpublished).

[30] R. Vogt, S. J. Brodsky, and P. Hoyer, Nucl. Phys. **B383**, 643 (1992).

[31] Z. Lin and M. Gyulassy, Phys. Rev. Lett. **77**, 1222 (1996).